THE ASTROPHYSICAL JOURNAL, 369:L75–L78, 1991 March 10

IONIZATION FRONTS AND SHOCKED FLOWS: THE STRUCTURE OF THE ORION NEBULA AT 0".1

J. JEFF HESTER,[1] R. GILMOZZI,[2,3,4] C. R. O'DELL,[5] S. M. FABER,[6] BEL CAMPBELL,[7] ARTHUR CODE,[8] DOUGLAS G. CURRIE,[9] G. EDWARD DANIELSON,[10] S. P. EWALD,[2] EDWARD J. GROTH,[11] JON A. HOLTZMAN,[12] T. KELSALL,[13] TOD R. LAUER,[14] ROBERT M. LIGHT,[6] ROGER LYNDS,[14] EARL J. O'NEIL, JR.,[14] EDWARD J. SHAYA,[9] AND JAMES A. WESTPHAL[10]

Received 1990 October 17; accepted 1990 November 14

ABSTRACT

We present *HST* Wide-Field Camera images of a field in the Orion Nebula obtained in emission from [S II], Hβ, and [O II]. The morphology of the [S II] emission is markedly different from the other lines. While Hβ and [O II] are distributed fairly smoothly, [S II] is dominated by filamentary features with widths between 0".1 and 1" which sharply highlight ionization fronts moving into dense neutral material. These photoionization fronts act as probes of the structure of the cavity walls of this blister H II region. Their morphology indicates that while the surfaces into which they are moving are textured, subarcsecond clumps with high density contrast are uncommon. An exception is a bow shock–shaped ionization front seen along the face of a solar system–sized (0".6 = 270 AU) clump which is itself seen in extinction.

The field contains a number of HH objects and related structures, many of which were previously recognized as such, but whose complex structure is revealed here by the resolution of *HST*. These include M42 HH 1, which is seen to be an intricate structure of knots and filaments with a head-tail morphology. M42 HH 2 shows structure from both the shocked cavity walls and the shocked atomic outflow. M42 HH 5–7 break into numerous condensations with an appearance reminiscent of HH 7–11. All objects with a bow shock–shaped structure (i.e., M42 HH 1, 5, 7, and 10) show enhanced Hβ emission at the apex of the structure where the shock should be strongest. M42 HH 8 and 9 may be HH objects viewed face-on, or alternatively condensations photoionized by a nearby A or B star. Emission from [S II] traces shocks at the walls of an ionized jet apparently emanating from a star in a dark cloud. This cloud seen in extinction is coincident with H_2 Peak 1, which we propose is on the near side of the nebula.

Subject headings: nebulae: Orion Nebula — nebulae: structure — stars: formation

1. INTRODUCTION

The Orion Nebula (M42, NGC 1976), located at a distance of ~450 pc, is the closest bright H II region, and as such is the prototype for its class. The model of M42 has changed considerably with the accumulation of observational data in all wavelength regimes, and with the recognition of the "blister" phase of H II region evolution (e.g., Zuckerman 1973; Pankonin, Walmsley, & Harwit 1979; Peimbert 1982) as the period when H II regions are selectively best seen at optical wavelengths. In this standard model the photoionizing stars of the Trapezium cluster are located in an open cavity on the front face of a giant molecular cloud into which an ionization front is propagating.

Numerous imaging studies have been carried out (see Goudis 1982 and references therein) dating back to the original photograph by Henry Draper (1880). These studies reveal structure down to the limit imposed by astronomical seeing. Subarcsecond structure within the nebula has been proposed to explain a wide range of phenomena ranging from the low "filling factor" for optical line and radio continuum emission (e.g., Osterbrock & Flather 1959) to apparent turbulence in the velocity field. The recent radiographs of Yusef-Zadeh (1990) show structure at very small scales as well, although care should be taken before interpreting all of the features highlighted by a nonlinear edge enhancement algorithm as discrete physical structures. In addition, the physical scale lengths associated with many radiative and gasdynamic processes are significantly less than the 10^{16} cm resolution limit imposed by normal ground-based seeing.

In the present *Letter* we present initial results from images of M42 obtained with the *HST* Wide-Field Camera. Even given its impaired performance, *HST* allows us for the first time to visually explore the structure of an H II region on size scales of 0".1 = 45 AU = 6.7×10^{14} cm.

[1] Infrared Processing and Analysis Center, California Institute of Technology, Pasadena, CA 91125.
[2] Space Telescope Science Institute, Baltimore, MD 21218.
[3] Also Astrophysics Division, Space Science Department, ESA.
[4] On leave from Istituto di Astrofisica Spaziale, CNR, Frascate.
[5] Department of Space Physics and Astronomy, Rice University, PO Box 1892, Houston, TX 7725.
[6] UCO/Lick Observatories, Board of Studies in Astronomy and Astrophysics, University of California, Santa Cruz, Santa Cruz, CA 95004.
[7] Physics Department, University of New Mexico, Albuquerque, NM 87136.
[8] Astronomy Department, University of Wisconsin—Madison; postal address: Washburn Observatory, University of Wisconsin, Madison, WI 53706.
[9] Department of Physics and Astronomy, University of Maryland, College Park, MD 20742.
[10] Division of Geology and Planetary Science, California Institute of Technology, Pasadena, CA 91125.
[11] Physics Department, Princeton University, Princeton, NJ 08544.
[12] Lowell Observatory, Flagstaff, AZ 86001.
[13] NASA/Goddard Space Flight Center, Code 685.0, Greenbelt, MD 20771.
[14] National Optical Astronomy Observatories, Tucson, AZ 85726.

2. OBSERVATIONS AND DATA REDUCTION

Images of a field in M42 were obtained with the Wide-Field Camera (WF) during the Orbital Verification phase of the *HST* mission through a number of narrow-band filters including F375N ([O II] λλ3726, 3729), F487N (Hβ λ4861), and F673N ([S II] λλ6717, 6731). All exposures were 600 s. The field observed is shown in Figure 1 (Plate L22). The data were flat-fielded using on-orbit flats in nearby broad-band filters (F336W for F375N, F439W for F487N, and F555W for F675N). While some residual flat-field structures persist in the flattened data, they are generally at a lower level than the structures observed in the nebula. Exceptions to this are a number of small chip features which are extremely color-sensitive and are especially prominent as "extra stars" in WF3. Low spatial frequency errors due to variations in transmission across the faces of the narrow-band filters are also likely. Cosmic rays were identified using a high-pass filter, then interpolated over.

These data pose a particularly difficult problem for image deconvolution. The only PSFs available for the WF at these wavelengths were theoretical on-axis PSFs computed for each camera and wavelength (Burrows et al. 1991). However, since the science objectives demanded that the entire field be processed, the biggest difficulty arose from the significant variability of the PSF across the field of the WF (Holtzman et al. 1991). Optimal deconvolution of sharp features also unacceptably amplified noise peaks in the diffuse (S/N = 20:1–40:1) background. After examining intermediate results obtained using up to 100 iterations of Lucy (1974) deconvolution, it was decided that the best compromise between enhancement of sharp features and excessive amplification of background noise and variations in the PSF was obtained after a modest 15 iterations. This enhanced the contrast of structures smaller than about 2″ at the expense of a moderate increase in graininess of the background and some *loss* of spatial resolution for the sharpest features. The effect of PSF variability is most noticeable for bright stars, where deconvolution enhances structure different from the model, while removing signal from adjacent regions. All features discussed below are readily apparent in the unprocessed data.

3. RESULTS AND DISCUSSION

Figure 2 (Plate L23) shows a color composite of the three frames with [S II] in red, Hβ in green, and [O II] in blue. An assortment of enlarged fields, including an example of a region before and after deconvolution, is shown in Figures 3 and 4 (Plates L24 and L25). The most striking aspect of these images is that while Hβ and [O II] are fairly smooth on scales less than a few arcseconds ($\sim 10^{16}$ cm), the [S II] emission shows significant structure to the limit of resolution of the image. Generally speaking, while all three lines tend to be brighter or fainter in the same regions, the Hβ and [O II] images are "fuzzier" than [S II]. Examples of sharp [S II] features include the two vertical lines seen in Figures 3 and 4*b*, and the filament on the right side of Figure 4*a*. This filament, together with the diffuse emission immediately to its right, has the appearance of a smoothly curving limb-brightened surface. Extinction features are seen throughout the field, ranging from "wormlike" features as small as 0.″5 across to much larger structures apparent in ground-based images, and are frequently bordered by [S II] emission. These data graphically show the extent to which it *cannot* be assumed that the physical conditions in the regions which dominate [S II] emission are at all like those in the regions which dominate emission in other lines.

3.1. *A Curtain of* [S II] *Emission: Tracing the Ionization Front–Photodissociation Region Boundary*

With the exception of a number of discrete features such as those discussed below, the [S II] emission is characterized by coherent, filamentary structures intermingled with more diffuse emission. This diaphanous morphology seems consistent with large but irregular curtains or sheets of emission with an intrinsic thickness between $\lesssim 6 \times 10^{14}$ cm and 10^{16} cm. Within the context of the blister model, we interpret these sheets as tracing the location of ionization fronts moving into the walls of the cavity and the surfaces of dense neutral or molecular clouds which remain within the interior of the H II region.

The interior of a blister H II region is highly ionized and relatively low density, so the direct stellar radiation field will be essentially unattenuated, at least for wavelengths primarily responsible for ionizing H, O I, and S I. In this case most of the opacity to ionizing photons occurs at the walls of the cavity, where the energy deposited by UV photons drives a photoevaporative flow. The density and pressure profile of this flow away from the cloud face must be a self-consistent structure in which the pressure gradient away from the cloud drives off material at the rate appropriate for the energy input from photons. This structure should be very similar to the case for evaporation driven by thermal conduction (e.g., Cowie & McKee 1977), in which the flow velocity may be supersonic.

In such a flow, emission from a given ion should peak in the highest density region within the flow where that ion is prevalent. Lines from high-ionization species such as [O III] will originate farthest from the dense wall. Emission from [O II] should peak closer to the wall, both because of the higher density there and because this region is shielded from photons capable of ionizing beyond O II by the outer regions of the flow (cf. Dopita, Dyson, & Meaburn 1974). Recombination radiation from H should originate throughout the [O II] and [O III] zones but should be brightest from the [O II] zone. Photons capable of ionizing species with IP < 13.6 eV (e.g., S I) penetrate beyond the edge of the H II region per se, where they form a photodissociation region (e.g., Tielens & Hollenbach 1985 and references therein). Emission from [S II] peaks in the very narrow zone at the interface between the H II region and the photodissociation region where the product of the climbing $n_{S\,II}$ and the dropping n_e is the maximum.

This picture fits the data very well. Offsets between unresolved [S II] features and their progressively more diffuse Balmer line and [O III] counterparts are frequently seen in ground-based imagery of H II regions (Hester et al. 1991). The sharpness of the [S II] fronts as seen in the WF/PC image shows that the edge of the ionization front is very abrupt, with a thickness typically between $\lesssim 10^{15}$ and 10^{16} cm. The factor of 10 variation in the width of the [S II] zone could reflect variations in the density of the cloud being evaporated, since the scale lengths of the effects discussed above are shorter at higher densities.

The coherence of the filamentary [S II] emission over many arcseconds ($\gtrsim 10^{17}$ cm) indicates that these fronts are generally moving into structures that are large compared to the scale of the front itself, rather than into small clumps of material. This argues against the suggestion (e.g., Castaneda & O'Dell 1987) that peculiar velocities of a ubiquitous population of unresolved knots might explain apparent "turbulence" seen in

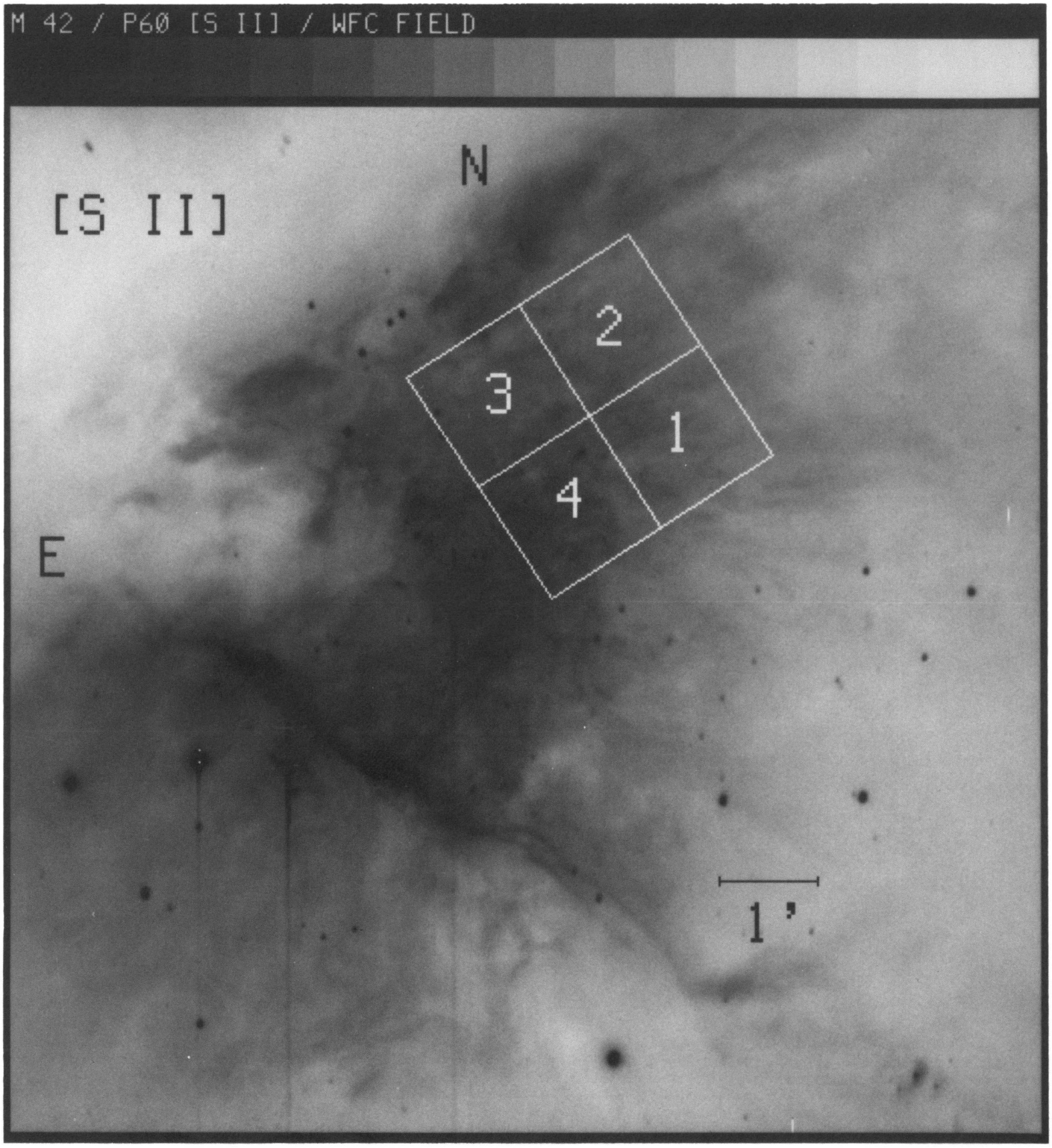

FIG. 1.—A ground-based [S II] image of the Orion Nebula obtained with a CCD camera on the 1.5 m telescope at Palomar Observatory. The region observed with the Wide-Field Camera is shown. The numbers indicate the identity of the four chips, referred to as WF1–4.

HESTER et al. (see 369, L76)

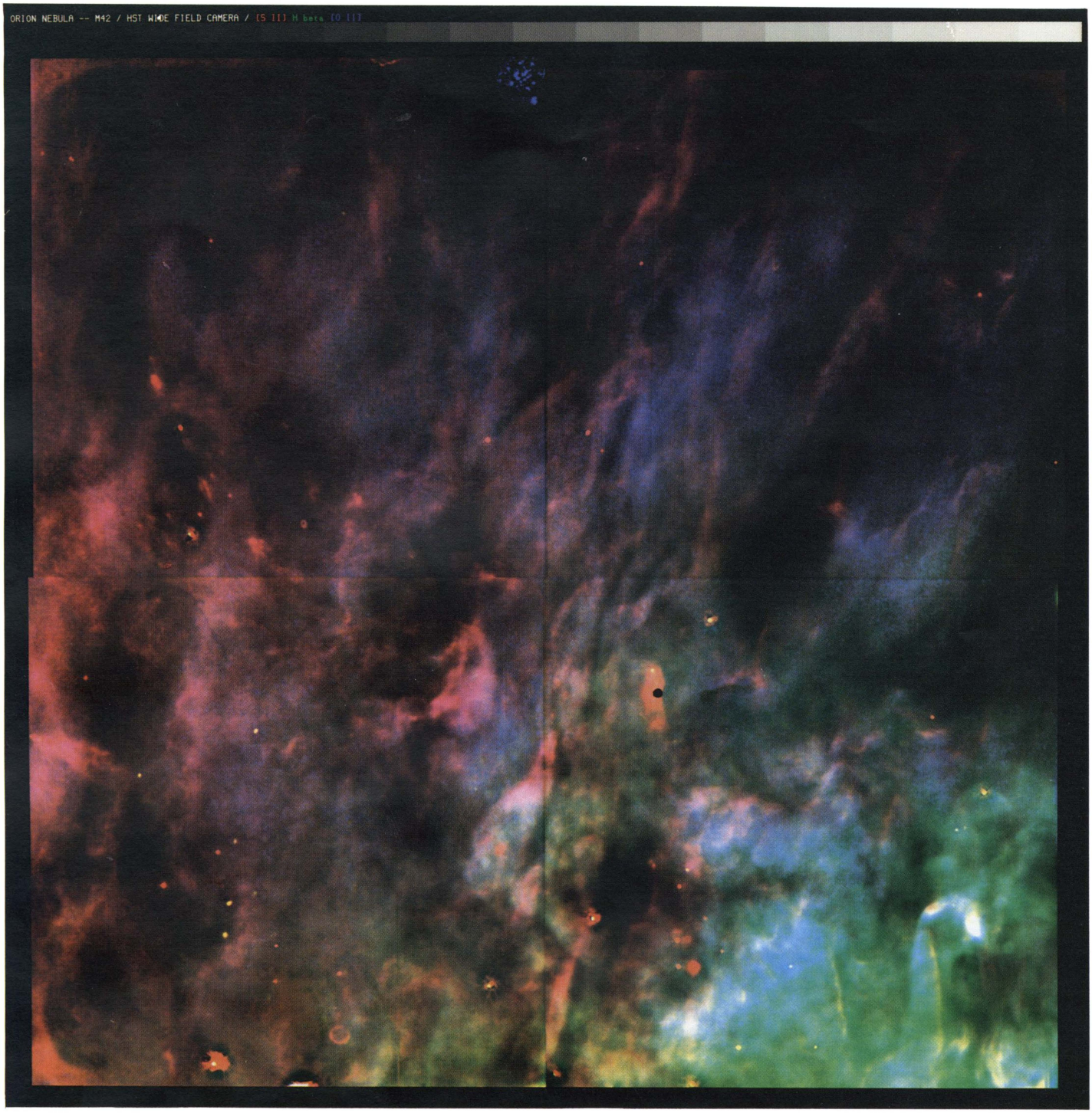

FIG. 2.—A color composite image of the entire field with [S II] $\lambda\lambda$6717, 6731 in red, Hβ in green, and [O II] $\lambda\lambda$3726, 3729 in blue. Modest processing has been applied to the indivudal frames (15 iterations of Lucy 1974 deconvolution). Residual structure around bright stars is due to variability of the point-spread function across the field of view of a chip. All four chips have been combined to produce the figure. All images were divided by the square root of the Hβ image after convolving that image with a 400 pixel FWHM Gaussian kernel. This reduces the dynamic range for display purposes, maintaining the sense of variations in the background level while allowing both fainter and brighter features to be seen. The chip order is WF1–4, beginning in the upper right corner and proceeding counterclockwise. The full field is $\sim$2.'55 on a side. The Baum Spot is visible in WF4 to the lower right of the field center.

HESTER et al. (see 369, L76)

PLATE L24

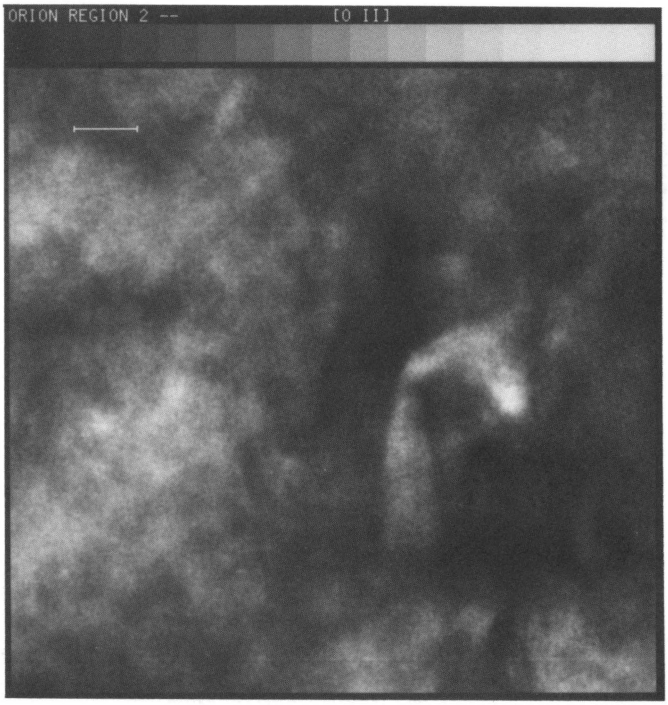

FIG. 3*a*

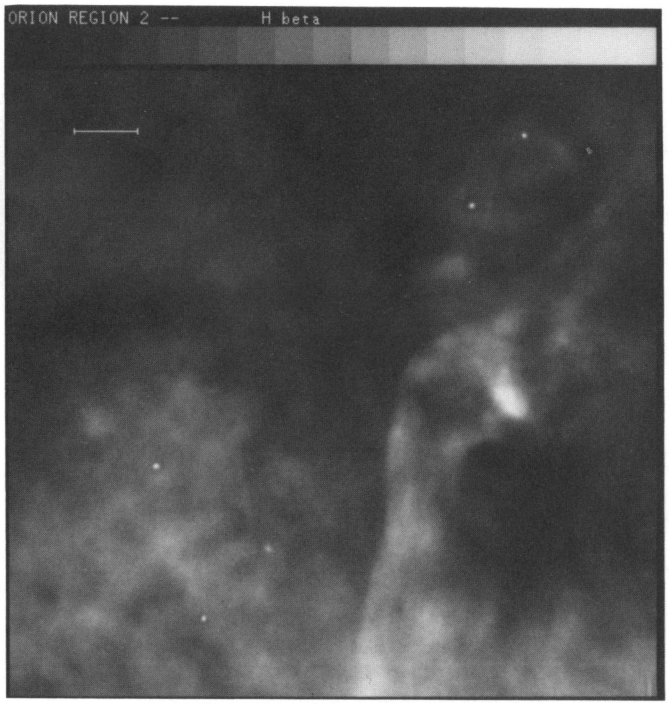

FIG. 3*b*

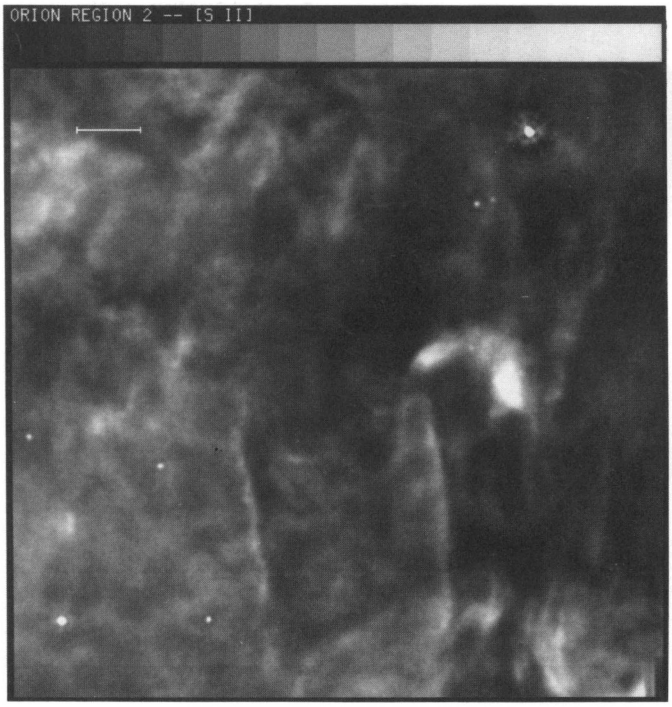

FIG. 3*c*

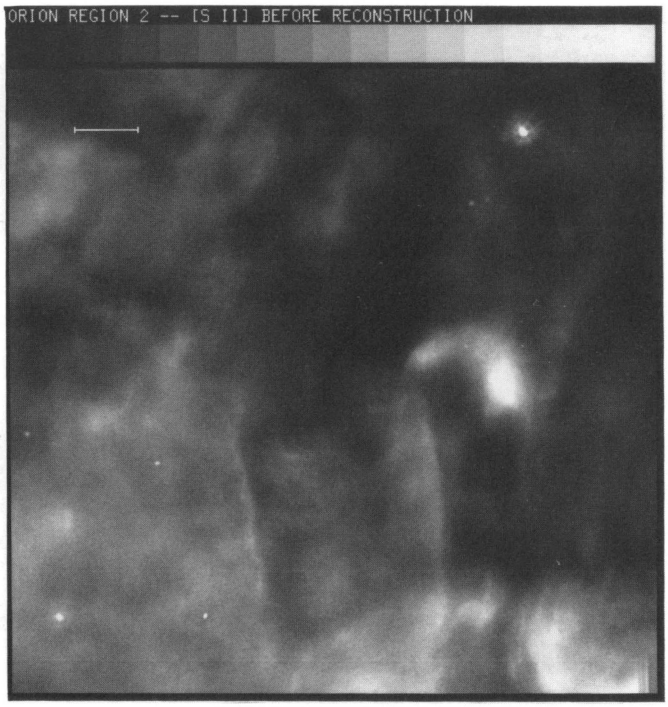

FIG. 3*d*

FIG. 3.—A blowup of a region in the lower right-hand corner of the field. Figures (*a*)–(*c*) show the processed [O II], Hβ, and [S II] images, respectively. The [S II] image, after flattening and cosmic-ray removal, but before deconvolution, is shown for comparison purposes in (*d*). The tick mark indicates 5″ = 225 AU at a distance of 450 pc. M42 HH 2 is located at the top of the "snorkel" in the lower right corner of the region. The vertical [S II] features are also discussed in the text.

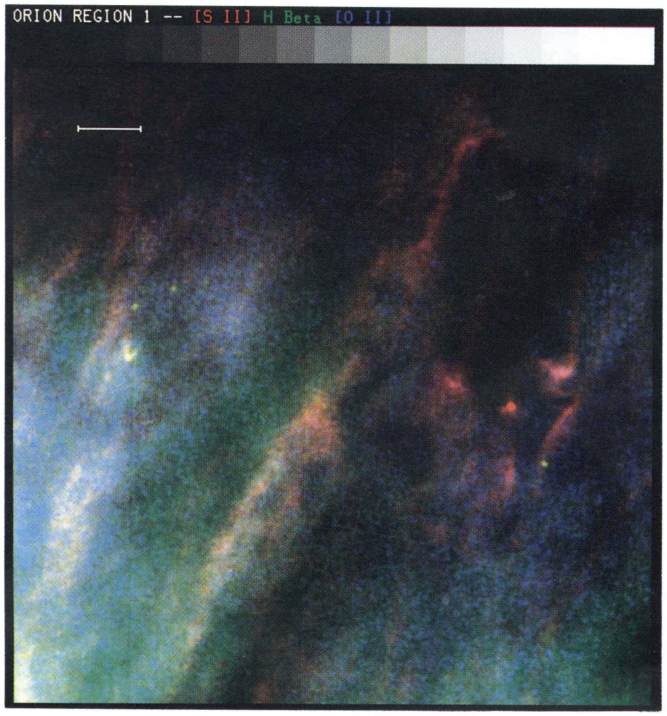

FIG. 4*a*

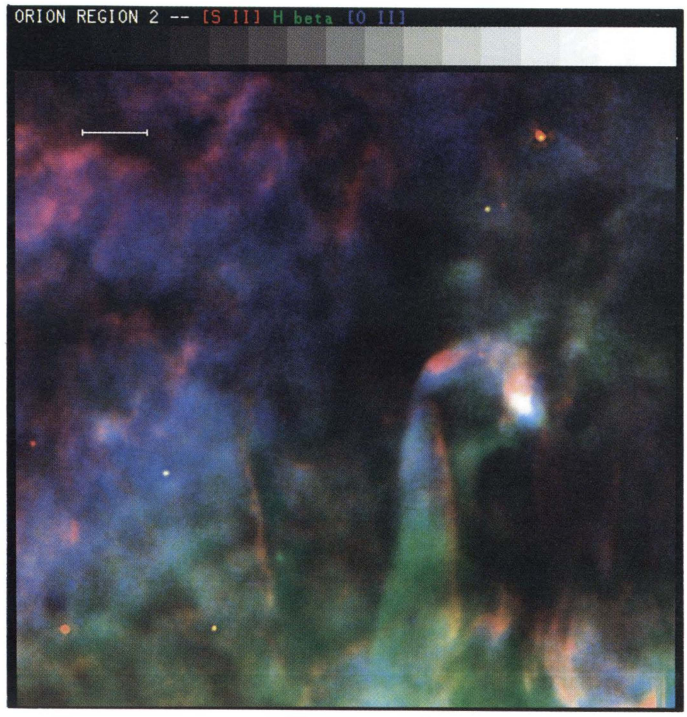

FIG. 4*b*

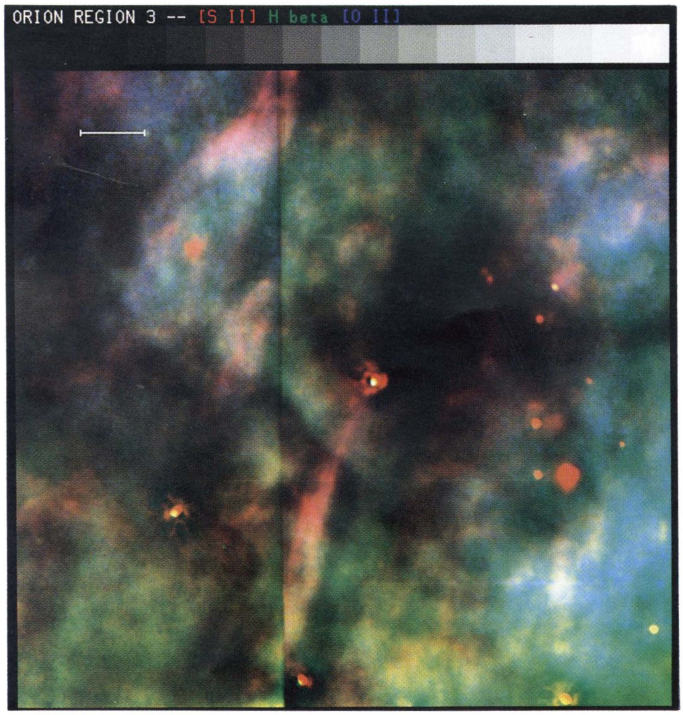

FIG. 4*c*

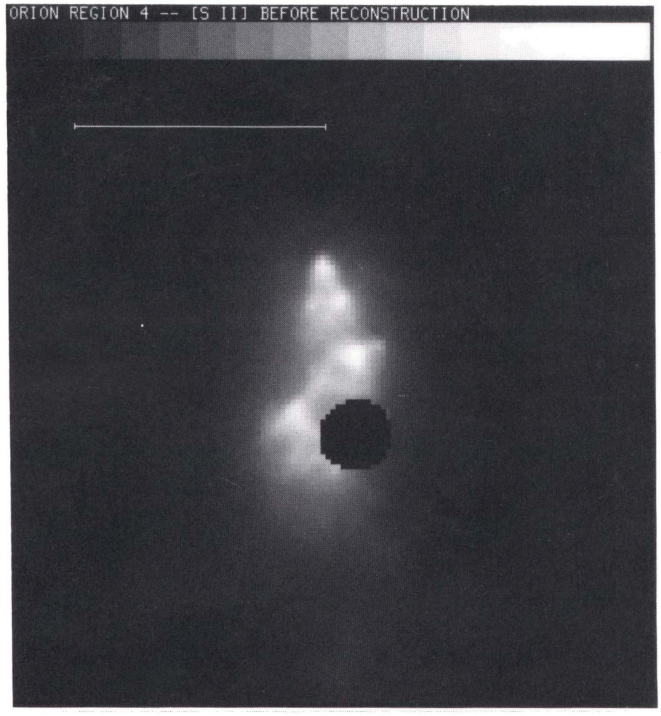

FIG. 4*d*

FIG. 4.—Blowups of several regions within the field. The color scheme for images (*a*)–(*c*) is [S II] in red, Hβ in green, and [O II] in blue. All tick marks show 5″. (*a*) The region in WF1 containing an ionization front being driven into a dense clump as well as an example of a sharp [S II] ionization front. (*b*) The region in WF4 for which individual line images are shown in Fig. 3. The two brightest knots constitute M42 HH 2. (*c*) The region around a prominent jetlike structure emanating from a star and a dark cloud coincident with H_2 Peak 1. The limb-brightened [S II] emission surrounding the center-filled Hβ is interpreted as radiative shocks along the walls of an ionized flow. M42 HH 8 and 9 appear as bright red knots to the upper right and lower left of the image. (*d*) The undeconvolved [S II] image of M42 HH 1 is shown because for these bright pointlike sources 15 iterations of Lucy deconvolution actually degrades the resolution somewhat. Note that the scale is a factor of 4 greater than (*a*)–(*c*). The round dark region is the Baum Spot.

kinematic data (although the smoothing caused by the PSF must temper this conclusion). As an alternative we point out that ordered flows together with variations in the geometry of the surface on scales smaller than the resolution limit can give the appearance of turbulence when none is actually present (cf. Hester 1987; Raymond et al. 1988).

3.2. *The Photoionization Front of a* 300 AU *Clump*

Figure 4*a* shows a blowup of a region of WF1. To the left side of this field is a small bow shock–shaped feature, $\sim 0\farcs6$ ($= 270$ AU $= 4 \times 10^{15}$ cm) in size. This structure is pronounced in both [S II] and Hβ. The [O II] image shows only an elongated depression coincident with the center of the feature. This depression can also be seen in the other images. The [S II]/Hβ ratio varies by about a factor of 2 around the nose of the structure and is a minimum along the edge which faces the cluster directly.

This object appears to be a very compact clump of material being photoevaporated by the UV illumination from the Trapezium. While we cannot rule out shock excitation, the strong Hβ emission as compared with the shocked structures below favors photoionization. The clump is ionized along the face pointing toward the cluster and not around its entire periphery, showing that the direct radiation field is still dominant at a distance of $\gtrsim 0.4$ pc from the O stars. One interpretation for this object is a dense core that existed before the evolving H II region dispersed the less dense material in which it was embedded. The pressure of the H II region may have been instrumental in forming the small clump from a larger structure. Assuming the temperature inside the clump to be ~ 100 K, the sound crossing time over which the clump should come into pressure equilibrium with its surroundings is of order 300 AU/1 km s^{-1} = 1500 yr, which is short compared to the lifetime of the clump.

This clump may be similar to the continuum radio sources nearer to the Trapezium observed by Moran et al. (1982), Garay, Moran, & Reid (1987), and Churchwell et al. (1987). Suggested interpretations for these objects range from externally photoionized globules to ultracompact H II regions with internal sources of ionization. Garay et al. (1987) preferred the earlier interpretation for a number of the objects they detected, and proposed a similar scenario to that above. The present data suggest that at least for this object the interpretation as a dense externally ionized clump is correct.

The depth of the extinction feature seen in [O II] at this location is hard to judge both because of smearing caused by the PSF and ambiguities with foreground and background emission; the data require at least a factor of 2 extinction in the clump and are consistent with a totally opaque object. Using standard values for E_{B-V} and R and taking a factor of 2 obscuration as a lower limit gives $n_{\rm H} > 4.5 \times 10^5$ cm^{-3} and $m > 1.2 \times 10^{-5}\ M_\odot$ for the clump. These may not be very interesting limits. Following the arguments from Garay et al. (1987) and scaling the radiation field by a factor of 100 ($1/r^2$ with $\tau = 0$) suggests $m > 3 \times 10^{-4}\ M_\odot$ for the clump to survive for the 3×10^5 yr age of the Trapezium stars. However, a clump with a mass closer to $10^{-5}\ M_\odot$ could have survived if it was uncovered within the last 10^4 yr.

3.3. *HH Objects and Related Structures*

The field observed includes a number of features which have been identified from the ground as HH objects (Gull et al. 1973; Canto et al. 1980; Axon & Taylor 1984) but about which very little structural information is available. In this section we briefly discuss these objects and their morphology. A more thorough discussion is beyond the scope of this *Letter* but will be presented in a subsequent paper.

3.3.1. *M42 HH 1 and 2*

M42 HH 1 appears in the upper left of WF4, unfortunately partially obscured by the Baum Spot. This is the brightest [S II] emission in the field by a factor of >2. Figure 4*d* shows an enlargement of the [S II] image of this structure. The object has a head-tail morphology, and is seen to break into a complex of bright [S II] knots joined by a network of filaments. Fainter filaments connect the bright portion of the object with a fainter condensation 5″ below the Baum Spot. This second condensation is coincident with a faint visible star and a 2 μm source in the map of McCaughrean published by Genzel & Stutzki (1989) and is a possible exciting source for M42 HH 1.

The Hβ morphology of M42 HH 1 differs markedly from its appearance in [S II]. A faint Hβ arc bounds the right side of the object, while the strongest feature in Hβ is the knot at the apex of the structure. The Hβ/[S II] ratio at this location is a factor of ~ 2.5 higher than for the second most prominent Hβ knot. This structure—with Hβ strongest relative to [S II] at the tip of a roughly conical structure—is likely due to the higher pressure at the point where the outflow strikes the end of its cavity (e.g., Stapelfeldt et al. 1991; Hartigan, Curiel, & Raymond 1989).

M42 HH 2 consists of the two bright knots at the top left and center right of the snorkel-shaped structure in Figures 3 and 4*b*. Canto et al. (1980) proposed that this HH object is due to an obscured star with a wind cavity that has broken out of the neutral filament seen in extinction. McCaughrean's 2 μm image shows a source located at the center of the loop at the end of the "snorkel." At *HST* resolution, the [S II] emission from the top component of M42 HH 2 is seen to consist of a small but resolved knot $\sim 0\farcs3$ across, which lies $0\farcs5$ inside of a moderately bright arc with an extent of $2\farcs5$. This arc forms part of the top of the "snorkel." A peak of Hβ emission located $0\farcs6$ inside of the [S II] peak can be explained by a model in which the [S II] emission comes primarily from a slow shock driven into the dense wall of the cavity, while Hβ comes predominately from the standoff shock in the flow (cf. Hartigan 1989; Stapelfeldt et al. 1991). The other component of M42 HH 2 is an elongated feature which is brighter in [S II] toward the top and brighter in Hβ toward the bottom.

3.3.2. *M42 HH 8 and 9*

M42 HH 8 and 9 can be seen in Figure 4*c* as two bright [S II] knots in the lower right and upper left parts of the figure, respectively. M42 HH 9 is resolved into two knots $0\farcs7$ apart between which lies a linear feature $1\farcs5$ long oriented perpendicular to the separation between the knots. M42 HH 8 is a resolved centrally concentrated [S II] knot about $1\farcs5$ across. An Hβ and [O II] extinction feature coincident with M42 HH 8 indicates that it may be a fairly massive object.

The one-sided velocity profile observed by Axon & Taylor (1984) and the fact that Jones & Walker (1985) should have been able to detect these objects but report no proper motion for them could be explained if these were HH objects viewed face-on. Alternatively, apart from their low ionization, these objects and a number of other [S II] features in this vicinity may be more similar to the "Partially Ionized Globules" studied by Dopita, et al. (1974) or the small continuum radio sources discussed above. In order to explain the brightness of

these objects and the flow speeds observed would require a source of soft ($E < 13.6$ eV) but intense radiation, such as a nearby A or B star.

3.3.3. *M42 HH 5, 6, 7, and 10*

The M42 HH 5, 6, and 7 system, visible in the lower left of WF2 in Figure 2, consists of at least six or seven discrete complexes of [S II] emission. M42 HH 5 (the topmost feature in the system) is bounded on the top by an Hβ arc. M42 HH 7 (the bottommost feature) is a pyramid-shaped complex of six knots with an Hβ-bright knot at its apex. A number of additional elongated [S II] knots seen to the lower left of this system appear to be HH objects as well.

M42 HH 10 is just at the left edge of WF3. It is also a cone-shaped structure consisting of a number of knots and filaments, and with a number of fainter "streamers" trailing off behind it. As with M42 HH 1, 5, and 7 (i.e., all of the HH objects in the field with shapes suggestive of a flow terminus), the knot at the apex of M42 HH 10 has a higher Hβ/[S II] ratio, tracing the point in the structure where the pressure is greatest and the shocks are strongest.

3.3.4. *A Shocked Jet from* H_2 *Peak 1*

The most prominent dark cloud in the field lies near the left edge of WF4, and is coextensive with a strong system of shocked H_2 emission ("Peak 1"; Beckwith et al. 1978). Figure 4*c* shows a 20″ long jetlike feature apparently emanating from a star located at the edge of this cloud. This jet bisects a wedge of weak extinction which also has its apex at the star. While a physical relationship between this feature and the star or the cloud cannot be proved on the basis of the images alone, the morphology strongly suggests that such a relationship exists.

In [S II] the jet is resolved into two filaments which bound a single linear feature 0.″5–2″ wide seen in [O II] and Hβ. We suggest that this jet is an outflow from Peak 1, perhaps from the visible star itself, and that the [S II] emission is coming from shocks at the interface between the jet and the material surrounding it. The extinction surrounding the jet could be due to a denser flow within which the jet is embedded. If the star is embedded in the dark cloud, then it may be visible only by virtue of our perspective looking down the length of the jet. The jet lines up fairly well with M42 HH 1, and if the flow is bipolar, this is a possible excitation source for that object as well.

We propose that Peak 1 is on the front face of M42 and is probably related to the portion of the molecular cloud known to stick out in front of the nebula along the line of sight. This jet provides evidence that star formation in Peak 1 is important in exciting outflows and outflow related phenomena in the area.

4. CONCLUDING REMARKS

Many other noteworthy features exist in these first visual images of an H II region with a resolution of $\lesssim 10^{15}$ cm. However, while these data do begin to fulfill the promise of *HST* for examining our local interstellar environment at physically interesting scales, they also serve to remind us of the limitations imposed by the compromised optical performance of *HST*. Even at the extremely high surface brightness of the Orion Nebula, the signal-to-noise ratio is much lower than one would like for deconvolution especially since small-scale structures are diluted by the PSF while the bright diffuse emission in which they are embedded is not. Further, while we feel comfortable at this point with morphological comparisons of the sort presented, it is dangerous to attempt to draw quantitative conclusions from deconvolutions of low signal-to-noise ratio images of morphologically complex structure. WFPC II will bring a factor of 5 improvement in sensitivity to structure of this sort, and we are left wondering what other remarkable objects lie just beyond our current reach.

J. J. H. would like to acknowledge numerous conversations on the structure of H II regions with R. J. Dufour and R. A. R. Parker, and with K. Stapelfeldt and J. Raymond on the structure of HH objects. J. J. H. acknowledges support from NASA and CIT through IPAC. The WF/PC IDT is supported by NASA contract NAS5-25451.

REFERENCES

Axon, D. J., & Taylor, K. 1984, MNRAS, 207, 241
Beckwith, S., S. E., Neugebauer, G., & Becklin, E. E. 1978, ApJ, 223, 464
Burrows, C., et al. 1991, ApJ, 369, L21
Canto, J., Goudis, C., Johnson, P. G., & Meaburn, J. 1980, A&A, 85, 128
Castaneda, H. O., & O'Dell, C. R. 1987, ApJ, 315, 55
Churchwell, E., Felli, M., Wood, D. O. S., & Massi, M. 1987, ApJ, 321, 516
Cowie, L. L., & McKee, C. F. 1977, ApJ, 211, 135
Dopita, M. A., Dyson, J., & Meaburn, J. 1974, Ap&SS, 28, 61
Draper, H. 1880, American J. Sci., 10, 388
Garay, G., Moran, J. E., & Reid, M. J. 1987, ApJ, 314, 535
Genzel, R., & Stutzki, J. 1989, ARA&A, 27, 41
Goudis, C. 1982, The Orion Complex: A Case Study of Interstellar Matter (Dordrecht: Reidel)
Gull, T. R., Goad, L., Chiu, H.-Y., Maran, S. P., & Hobbs, R. 1973, PASP, 85, 526
Hartigan, P. 1989, ApJ, 339, 987
Hartigan, P., Curiel, S., & Raymond, J. 1989, ApJ, 347, L31
Hester, J. J. 1987, ApJ, 314, 187
Hester, J. J., Dufour, R. J., Parker, R. A. R., & Scowen, P. 1991, An Atlas of H II Region Ionization Structure (NASA Special Publication), in preparation
Holtzman, J., et al. 1991, ApJ, 369, L35
Jones, B. F., & Walker, M. F. 1985, AJ, 90, 1320
Lucy, L. B. 1974, AJ, 79, 745
Moran, J. M., Garay, G., Reid, M. J., Genzel, R., & Ho, P. T. P. 1982, Ann. NY Acad. Sci., 395, 204
Osterbrock, D. E., & Flather, E. 1959, ApJ, 129, 26
Pankonin, V., Walmsley, C. M., & Harwit, M. 1979, A&A, 75, 34
Peimbert, M. 1982, Ann. NY Acad. Sci., 395, 24
Raymond, J. C., Hester, J. J., Cox, D. P., Blair, W. P., Fesen, R. A., & Gull, T. R. 1988, ApJ, 324, 869
Stapelfeldt, K. R., Beichman, C. A., Hester, J. J., Scoville, N. Z., & Gautier, T. N. 1991, ApJ, in press
Tielens, A. G. G. M., & Hollenbach, D. 1985, ApJ, 291, 747
Yusef-Zadeh, F. 1990, ApJ, 361, L19
Zuckerman, B. 1973, ApJ, 183, 863